UPPSALA
UNIVERSITET

Numerical modelling of positive electrical discharges in long air gaps

OSCAR DIAZ

Dissertation presented at Uppsala University to be publicly examined in Polhemsalen, Ångström Laboratory, Lägerhyddsvägen 1, Uppsala, Thursday, 15 September 2016 at 10:00 for the degree of Doctor of Philosophy. The examination will be conducted in English. Faculty examiner: Ph.D. Raul Montano (R&D Manager PG/PT ABB AB).

Abstract
Diaz, O. 2016. Numerical modelling of positive electrical discharges in long air gaps. *Digital Comprehensive Summaries of Uppsala Dissertations from the Faculty of Science and Technology* 1389. 58 pp. Uppsala, Sweden: Acta Universitatis Upsaliensis. ISBN 978-91-554-9623-4.

This dissertation deals with research on the numerical modelling of electrical discharges in laboratory long air gaps excited with positive switching impulses. It begins with the preliminary work of several scientists during the last decades, making a detailed analysis of different approaches for modelling all the stages in a full discharge. The relations between these models are identified as well as the effect on the outcome when modifying some important input parameters.

The general concept describing the discharge phenomenon usually includes three main elements: the streamer inception, the streamer-to-leader transition and the stable leader propagation. These elements are present in many of the analysed models and the main differences between them are the assumptions and simplifications made by each author at a specific point in their methodologies. The models are usually simplified by assigning experimentally determined values to physical constants pertinent to different stages of the full discharge. These constants are the potential gradient in the leader-corona region to sustain the leader propagation, the charge per unit length along the leader channel which depends on the atmospheric conditions and the voltage impulse wave shape; and the leader propagation velocity, which is closely related to the discharge current. The dissertation includes the results of laboratory work related the study of leaders in long gap discharges, electrical parameters and optical records. By reconstructing the three-dimensional leader propagation for the rod-to-plane configuration, it was possible to study the random tortuous path followed by the leader as it propagates.

One important element included in the discharge modelling is the representation of the leader-corona region in front of the leader tip as it propagates towards the grounded electrode. For the calculation of the net charge available in the leader-corona region, two new methodologies were pro-posed based on the electrostatic potential distribution obtained from a finite element method solver. This allowed the inclusion of more elements representing different parts of the discharge in the simulation domain.

In the final part, all the analysed elements and the new proposed ones were included in a new methodology for the modelling of electrical dis-charges in long air laboratory gaps. The results obtained from this methodology were compared to experimental data. A good agreement was found between the simulation results and the experimental data.

Keywords: high voltage techniques, numerical modeling, electrical discharge in gases, streamer mechanism, leader channel

Oscar Diaz, Department of Engineering Sciences, Electricity, Box 534, Uppsala University, SE-75121 Uppsala, Sweden.

To new beginnings,
new things to live and learn,
to the miracle of life,
to my son David

List of Papers

This thesis is based on the following papers, which are referred to in the text by their Roman numerals.

I   **Diaz, O.**, Arevalo, L., Cooray, V., "Leader channel models for long air positive electrical discharges", *Journal of Electrostatics*, 76 (2015):208–215

II   **Diaz, O.**, Arevalo, L., Cooray, V., "Parameter variation in leader channel models used in long air gap discharge simulation", *Electric Power Systems Research*, 139 (2016):32-36
Paper II was presented at the 32nd International Conference on Lightning Protection ICLP, Shangai, China, 2014 (see Paper VII)

III   **Diaz, O.**, Hettiarachchi, P., Rahman, M., Cooray, V., Vayanganie, S., "Experimental study of Leader Tortuosity and Velocity in Long Rod-plane Air Discharges", *IEEE Transactions on Dielectrics and Electrical Insulation*, 23, 2 (2016):806-812

IV   **Diaz, O.**, Arevalo, L., Cooray, V., "Methodologies for the charge estimation in the leader corona region used in modeling long air gaps under positive voltage impulses", *Proceedings of the 33rd International Conference on Lightning Protection (ICLP)*, Estoril, Portugal, 2016.

V   **Diaz, O.**, Arevalo, L., Cooray, V., "Numerical modeling of long air laboratory gaps tested with positive switching impulses", *submitted to the IEEE Transactions on Dielectrics and Electrical Insulation*, 2016.

A contribution and other papers of the author not included in this document:

VI   Vayanganie, S., Cooray, V., Rahman, M., Hettiarachchi, P., **Diaz, O.**, Fernando, M., "On the occurrence of 'Bead Lightning' Phenomena in Long Laboratory Sparks", *Physics Letters A*, 380 (2016): 816-821

VII   **Diaz, O.**, Arevalo, L., Cooray, V., "Sensitivity analysis of leader channel models used in long air gap positive discharge modelling", *Proceedings of the 32rd International Conference on Lightning Protection (ICLP),* Shanghai, China, 2014.

VIII   **Diaz, O.**, Becerra, M., Cooray, V., "Arc modeling for a low current impulse discharge in an enclosed microspark gap", *Proceedings of the 19th International Conference on Gas Discharges and their applications (GD),* Beijing, China, 2012.

IX   **Diaz, O.**, Cooray, V., "Effect of pressure on the electrode fall for impulse arcs in argon between copper electrodes", *Proceedings of the 30th International Conference on Phenomena in Ionized Gases (ICPIG),* Belfast, Northern Ireland, 2011.

X   **Diaz, O.**, Cooray, V., "Cold-electrode voltage fall for impulse arcs in argon between copper electrodes", *13th International Conference on Electrostatics, Journal of Physics: Conference Series,* 301 (2011) 012042

XI   **Diaz, O.**, Cooray, V., Schleimann-Jensen, J., "Electrode energy dissipation in a new flat low voltage surge protective gas discharge tube", *Proceedings of the 30th International Conference on Lightning Protection (ICLP),* Cagliari, Italy, 2010.

XII   **Diaz, O.**, Arevalo, L., Cooray, V., Mejia, A., "Electrical breakdown in soil under uniform background electric fields", *Proceedings of the International Conference on Grounding and Earthing GROUND'2010 and 4th International Conference on Lightning Physics and Effects (LPE),* Salvador, Brazil, 2010.

Reprints were made with permission from the respective publishers.

Contents

Nomenclature and abbreviations

DC	Direct current systems
AC	Alternating current systems
$U_{50\%}$	50% probabilistic breakdown voltage
HV	High Voltage
PDE	Partial differential equations
FEM	Finite element method
FACTS	Flexible alternating current transmission systems
HVDC	High Voltage direct current systems
LCR	Leader-corona region
SSI	Single surface integral method
CMM	Capacitance matrix method
CSM	Charge simulation method
CCD	Charge-coupled device image sensor for the fast camera
E/p	Electric field divided by gas pressure
E/N	Reduced electric field
N_{stab}	Stabilization charge
α	Ionization coefficient for electron avalanche in electrical gas discharges
η	Attachment coefficient for electron avalanche in electrical gas discharges
q_L	Electric charge per unit length for the leader channel advancement
E_{SC}	Constant electric gradient to sustain streamer discharge inside the LCR
ΔU_l	Potential drop along the leader channel
l_Z	Leader channel vertical length
E_∞	Leader gradient ultimate value
E_i	Leader gradient initial value
x_0	Space constant for the Rizk leader channel model
a_0, a	Leader channel radius, initial and last
N_0, N	Leader channel particle density, initial and last
γ	Constant ratio between specific heats
a_{j0}, a_j	Leader channel radius at the j-segment, initial and last
N_{j0}, N_j	Leader channel particle density at the j-segment, initial and last
U_{Ltip}	Potential at the leader tip
ΔQ_{SC}	Calculated charge step in the LCR, injected into the leader channel
x_L	Leader channel tip location for the Lalande-Goelian leader model

x_{SC}	Streamer front location (LCR limit), for the Lalande-Goelian leader model
K	Factor for the streamer number and geometry with the Lalande method for the calculation of ΔQ_{SC} in the LCR
K_Q	Factor for the calculation of the ΔQ_{SC} with the Becerra-Cooray method
dQ_j	Charge element for the calculation of the ΔQ_{SC} in the Arevalo method
C_{ij}	Capacitance matrix element, used for the estimation of ΔQ_{SC} with the CMM
ε_0	Vacumm permittivity

1. Introduction

The fast technological revolution of the 20th century would have not been possible without the development of bigger and more reliable energy systems. The progress, from the earliest DC transmission systems to the present-day AC/DC systems with hundreds of kilovolts, came with a continuous escalation in the requirements for the insulation systems. The use of external air insulation in most transmission lines and substations is closely linked to the perturbations and transients caused by lightning strikes and switching operations and the repercussions these have on all the elements interacting within the power grid.

To be able to design and build bigger and more robust power networks, one needed to understand and be able to predict all the physical phenomena involved in the electrical discharge. The first approaches relied mainly on laboratory testing. Different electrode configurations, resembling real cases, were tested to find out the 50% probabilistic breakdown voltage ($U_{50\%}$), both for fast and slow front voltage impulses. Most of the early theoretical work addressed small gap phenomena and electrical discharges considering different types of gases, electrodes, etc.

The improvement of the high voltage (HV) laboratory techniques and a better understanding of the phenomena involved in electrical discharges occurring in larger atmospheric air gaps, lead to an improved design of HV equipment and facilities. Consequently, the power systems became more reliable when operating at higher voltage levels.

During the last decades, the use of faster and more powerful computational resources allowed researchers to propose different and more complex methodologies to describe the long air gap electrical discharges. The methods range from models using a simplified representation of the discharge (such as an arrangement of electrical charges), to more complex models where the conservation of mass, momentum and energy equations for several species available in the atmospheric air are solved simultaneously with the electrostatic potential distribution.

This dissertation deals with the study of models available to represent the electrical discharge in laboratory long air gaps when tested with positive switching voltage impulses. It analyses the different stages of the electrical discharge as building blocks and the way these could be used or interchanged in the various methodologies to represent the full breakdown event.

1.1. State of the art

The study of electrical discharges dates back to observations made by our ancestors. They tried to understand the lightning phenomena present in nature. During the last two centuries, scientific knowledge has increased enormously and encompasses the electromagnetic theory and the detailed description of electrical discharges. As mentioned in the introduction, during the last decades the knowledge and understanding of long air gap electrical discharges has evolved with the growth of the electrical energy systems, and their requirement to provide uninterrupted energy transmission.

It would be too complex to mention all the contributions from scientists who have worked on electrical discharges, especially long air gap electrical discharges, in this thesis. Therefore, the time range was set to about 50 years, starting with the work of *Les Renardières* group [1–3]. The group's extensive research spanned more than a decade. It included rigorous laboratory work alongside theoretical work by scientists from different countries, who made important contributions [4–9] as well as by other scientists from different institutions [10–14].

All the stages involved in the long air gap are now fully recognized. However, there is still no absolute model that can represent accurately and simultaneously, all the physical phenomena and the transitions occurring between the stages in a full discharge [15]. Given the complexity of all the physical phenomena involved, proper assumptions must be made to simplify its representation.

The existence of more powerful computational resources permitted the implementation of more complete models to represent the phenomena taking place during the different stages of the electrical discharge. This includes the capability of solving larger systems of partial differential equations (PDE) for mass, energy and momentum equations, and their electromagnetic interaction.

There have been different approaches to explaining the whole electrical discharge in long air gaps. Some authors go into greater detail [9, 16], and others make assumptions to simplify their models [17–20]. Our research group's recent work on lightning attachment, is closely related to the modelling of long air gap discharges [21–24].

The current simulation techniques are computer based. The simulations are limited by the model complexity and the amount of available computational resource. The computational resource can stretch from personal computers to large clusters with hundreds of processors and memory and storage capacity in the several terabytes range. The use of Finite Element Method (FEM) solvers has facilitated the time demanding task of estimating the electrostatic potential distribution in the simulation domain, including all the elements used to represent the discharge geometry. The FEM solver can also be used to solve partial differential equations [25].

1.2. Research question and goals

The computer simulation has become a very important tool during the design processes in the industry. Most times, it can reduce costs during the product development. However, a simulation can also predict the behaviour of the whole physical system output by modifying some of its input variables, a task that in the real case scenario might be too complex. If the model used is set up consistently and validated properly, a simulation can be of great interest to research and development teams in several engineering applications.

For HV equipment, the new designs are oriented towards higher operative voltages imposed by the larger use of flexible alternate current transmission systems (FACTS) in combination with high voltage direct current (HVDC) systems. During the design stage, most costs arise from testing in large HV facilities. These have become rare and expensive during the last decades.

Consequently, this dissertation endeavours on the physics of the discharge and interpretation of laboratory results for the estimation of $U_{50\%}$ voltages for different electrode arrangements. The proposed new methodology considers a tortuous leader progression in a three-dimensional domain, which permits the study of non-symmetric geometries.

1.3. Thesis outline

Chapter 2 refers to the generalities of the positive long air gap discharge, presenting the different stages of the whole phenomenon.

In **Chapter 3**, the leader channel is analysed in detail, as it is one of the most important parts of the discharge. Some leader channel models proposed in literature were analysed in **Papers I** and **II**. Further work was devoted to the experimental study of the leader channel propagation, giving special attention to its tortuosity, which was reported in **Paper III**.

Chapter 4 presents a more general aspect of the simulation methodologies. Various models and methodologies were studied to represent the approaches of other authors.

Chapter 5 focuses on the different methodologies available to evaluate the amount of charge available in the leader corona region (LCR) in front of the leader tip as it propagates. Two new methodologies to do this estimation, the single surface integral (SSI) and the capacitance matrix method (CMM) were presented in **Paper IV**.

Finally, the results of using the new SSI and CMM methodologies and their implementation in a numerical model used to model non-symmetric geometries submitted for publication in **Paper V**, are presented in **Chapter 6**.

2. Generalities of the positive long laboratory air discharge

One of the most important contributions by *Les Renardières* Group [1–3] is to identify and analyse in detail the structure of the positive electrical discharge in long air gaps, tested with HV impulses. For the rod-to-plane electrode configuration, records of voltage, current, electric field and optical radiation were reported. Since this is one of the most commonly studied electrode configurations, the description presented on this section focuses on it. In the case of less sharp HV electrodes (larger tip radius), such as spheres or hemispheres, the main differences compared to the rod-to-plane configuration were also mentioned. Fig. 1 presents a general view of the positive electrical discharge.
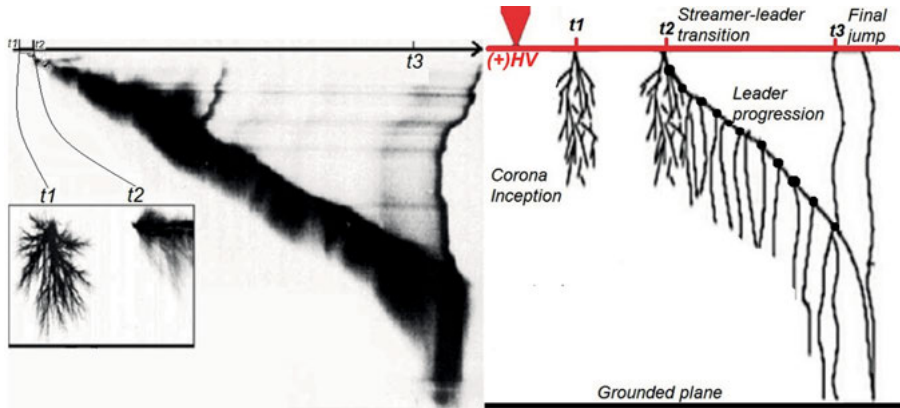

Figure 1. Streak image and schematic representation of a positive long air-gap discharge, occurring when testing a cone-to-plane electrode arrangement with a positive voltage switching impulses 500/2500 µs and U_{cr} = 2.5 MV (adapted from [26] with permission from the editor).

In general, the positive long air gap can be divided into three main stages: the streamer inception ($t1$), the streamer to leader transition ($t2$) and the leader progression that will eventually lead to a full breakdown ($t3$). A more detailed explanation of each stage is presented in the next subsections.

14

2.1. Streamer inception

The streamer inception, also known as the corona inception or first corona, is a direct consequence of ionization processes near the electrically stressed electrode, in a non-homogeneous electric field distribution. Once a free electron is able to initiate one avalanche, it can grow further if certain conditions are met. The conditions are mainly linked to the electric field intensity on the HV electrode. The availability of this free electron is a statistical process. As a consequence, it produces statistical time lags for the occurrence of the streamer inception for similar experimental conditions (geometry and electrical stimulus) [9].

Many authors use the Meek's criterion for streamer inception [27, 28]. Starting with Townsend's theory for avalanche discharge in atmospheric air, one finds a minimum amount of electrical charge in the avalanche head to sustain the streamer propagation. This stability charge is related to the ionization and attachment coefficients. These have been estimated experimentally for several gases as a function of the reduced electric field E/N or the electric field divided by pressure E/p [29]. The stabilization charge can be estimated by:

$$N_{stab} = e^{\int_{x_0}^{x_1}(\alpha-\eta)\cdot dx} \qquad (2.1)$$

where N_{stab} is the stabilization charge, α and η are the ionization and attachment coefficients respectively, in a way that more charges are produced than those that are lost, i.e. $\alpha-\eta > 0$. This condition is usually met when the total electric field (space charge plus background) in the ionization region, also known as the active region in the HV electrode vicinity, is higher than 26 kV/cm. Both coefficients are a function of the local E/N in a given region between x_0 and x_1 where the criterion is evaluated. In this simplified calculation, the effects of diffusion and charge distortion are disregarded. For atmospheric air, the minimum N_{stab} is found when [7, 30]:

$$\int_{x_0}^{x_1}(\alpha-\eta)\cdot dx \cong 18 - 20 \qquad (2.2)$$

Substituting these values in (2.1) one finds that N_{stab} varies between $6.5\cdot10^8$ and $4.8\cdot10^9$ ions. In experiments, the streamer inception has been observed as several streamer branches that originate from a common point on the electrode surface, as it can be seen at *t1* in Fig. 1. A current impulse is then recorded, with a rise time of 10 to 50 ns and 200 to 500 ns of tail time [9, 15].

2.2. Streamer-to-leader transition

The concept of streamer-to-leader transition, also known as leader inception or second corona, can be applied to the leader inception at the common stem of the streamers on the electrode surface. At the same time, it can be applied to the formation of a new leader section within the corona region [15], as presented in Fig. 1 for *t2*.

After streamer inception at t_1, there is a period of low radiation and reduction of injected charge, known as the dark period, which is influenced by the charge injected in the streamer inception, the electrode shape and the resultant electric field distribution. According to experimental results, the dark period becomes shorter for HV electrodes of large curvature and increases for sharper ones. This is due to the different amount and the distribution of the charge produced in the corona region after the streamer inception [2, 6, 9]. An example of a current record for a sharp electrode tested with a positive voltage switching impulses is presented in Fig. 2.
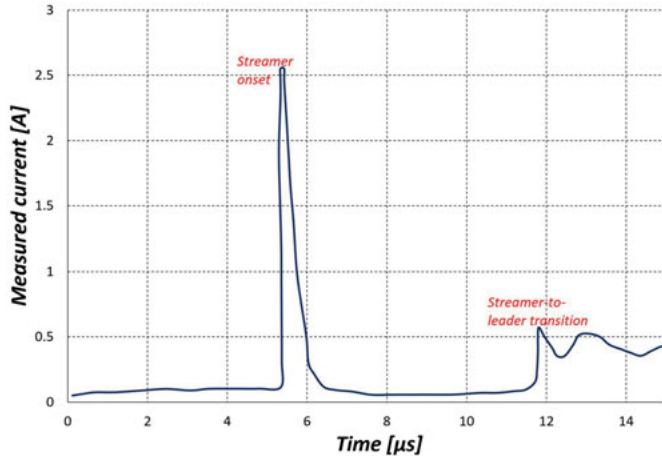

Figure 2. Streamer onset and streamer-to-leader transition when testing a cone-to-plane electrode arrangement with positive voltage switching impulses. Note the dark period of ca. 6 µs between the two current increments (experimental data adapted from *Les Renardières* group [9]).

The duration of the dark period has been associated with a critical radius on the HV electrode [2, 13], which depends mainly on the electrode geometry and the gap length. For a given radius below the critical value, the $U_{50\%}$ is constant, while having a different streamer inception and different streamer-to-leader transition voltages. In the opposite case, the $U_{50\%}$ increases with the equivalent radius and the streamer inception and the streamer-to-leader voltages tend to be the same (the dark period is almost zero).

An early approach to explain this transition was proposed by Aleksandrov [10]. He considered that all electrons produced in the streamer converged into a common stem. There they released energy by collisions with the neutral gas, which would eventually heat up the common stem of the streamer, increasing its conductivity and decreasing its internal electric field. Gallimberti [9] departed from this concept and proposed a more detailed thermo- hydro-dynamic model for the streamer-to-leader transition in atmospheric air. A minimum streamer corona charge of 1 μC is estimated to be necessary to heat the common stem above a critical temperature threshold which corresponds to the thermal detachment of negative ions (ca. 1500 – 2000 K) to build the first stage of the leader channel.

2.3. Leader propagation

Once the streamer processes in front of the stressed electrode have given way to the formation of the early leader channel stem, it will start to propagate if the streamer ionization at its tip is high enough to sustain the supply of charge. Records of the measurable physical variables in laboratory conditions are well documented and correspond with the theoretical analysis of the processes associated with leader propagation [1–3, 7, 9, 14]. A photograph of the growth and propagation of the leader channel can be seen in Fig. 3. One can see the channel and the leader-corona region (LCR) as a luminous cone in front of the leader tip as it propagates towards the grounded plane [26].

Figure 3. Frame photograph from a 10 m cone-to-plane electrode configuration tested with positive voltage switching impulses 500/10000 μs (adapted from [26] with permission from the editor).

For the switching voltage impulses (slow front), the effective propagation velocity remains between 10^4 and 10^5 m/s [31, 32] and the current at the channel base remains almost constant at 1 A. The leader current and velocity are related by the constant q_L. This constant represents the amount of electric charge required per unit length for the leader advancement, depending mainly

on the relative humidity, changing between 20 and 50 μC/m, for 12 and 5 g/m^3 respectively [2, 9, 18, 19, 26]. After the streamer-to-leader transition, the continuous propagation of the leader takes place in most cases until the LCR limit reaches the grounded plane. At this point the discharge most probably will reach the breakdown stage. The leader tip location at the moment when the LCR limit reaches the grounded plane is known as the final jump height. More detailed descriptions of the models available for the representation of the leader channel and the LCR are presented in Chapter 3 and 4.

3. Leader channel modelling

Among the experimental and theoretical work introduced in Chapter 2, various models to represent the leader channel have been proposed. Depending on the level of detail, they can be classified as the engineering type or the physical type. The engineering models combine the knowledge of the general physical discharge characteristics required to predict the $U_{50\%}$ and its statistical variation [7]. Physical models on the other hand base their calculations on the conservation of mass, momentum and energy, continuity of charged, neutral and excited species available during the discharge development coupled with basic electromagnetism. Additional information like the number and type of chemical reactions between different species, the temperature, channel radius, potential distribution, LCR limit and leader tip location in time and space, may be obtained as well.

3.1. Leader channel models

Both engineering and physical leader models were studied in **Paper I**. The engineering models studied were due to of Jones [7], Hutzler [33], Bazelyan [34] and Rizk [17, 35]. The physical models studied were due to Waters [3, 5, 7] and Gallimberti [3, 9], and the extension of the Gallimberti model by Lalande [18]. The assumption of a constant potential gradient required to sustain the streamer discharge E_{SC} in the LCR is widely utilized in both the engineering and the physical models, such as the models of Jones, Hutzler, Bazelyan, Waters, and Gallimberti/Lalande. At the same time, the constant charge per unit channel length q_L is assumed by Hutzler, Waters and Gallimberti/Lalande.

The mentioned models of Rizk and Lalande were analysed in a greater detail in **Papers II** and **VII**. The main element of the comparison was the potential distribution along the channel and at the leader tip. Some input constants from each model were modified and output variables like the extension of the LCR and the leader tip potential were examined.

The engineering model of Rizk is based on an electrostatic representation of the LCR and the leader channel by point electrical charges located at a certain distance from the electrode tip. The model shares common concepts from Jones [7] and Hutzler [33] for the leader gradient calculation. The potential distribution along the leader channel for a rod-to-plane electrode arrangement can be calculated as a function of the channel length l_Z (3.1):

$$\Delta U_l = l_z \cdot E_\infty + x_0 \cdot E_\infty \cdot ln\left[\frac{E_i}{E_\infty} - \frac{E_i - E_\infty}{E_\infty} \cdot e^{-l_z/x_0}\right] \qquad (3.1)$$

where E_i and E_∞ are the initial and ultimate values of the leader gradient. x_0 is a space constant estimated by $x_0 = v_L \cdot \Theta$ (v_L being the leader propagation average speed and Θ a time constant with value $\Theta = 50$ μs).

The physical thermo- hydro-dynamic model of Gallimberti [3, 9] is a simplified non-local thermal equilibrium model for a weak shock. The model assumes that the channel can be represented as a homogeneous cylinder surrounded by a dense shell. Over the channel cross section, the pressure, temperature and particle density remain constant. Starting from the energy balance for the channel core and shell, the model is able to evaluate the channel radius (3.2) and the potential drop along the channel, assuming a constant amount of mass that behaves like an ideal gas (3.3):

$$\pi a^2 = \sqrt{(\pi a_0^2)^2 + 2\frac{\gamma\text{-}1}{\gamma} \cdot \frac{E}{N} \cdot \frac{N_0 \cdot \pi a_0^2}{p} \cdot q_L \cdot \Delta x_L} \qquad (3.2)$$

Where N, N_0 and a, a_0 are the radius and particle density at times t and t_0, respectively, γ is the constant ratio between specific heats ($\gamma = c_p/c_v$), E is the internal channel electric field, p is the gas pressure, Δx_L is the distance the leader tip has travelled during the period of time t_0 to t. Thus, the new radius a, at a location x_L along the leader channel, results from the expansion of the initial radius a_0. By integrating the electric field in (3.2), the potential drop along the leader channel is calculated (3.3).

$$\Delta U_L(x_L) = \frac{\gamma}{\gamma\text{-}1} \cdot \frac{p \pi a_0^2}{q_L} \cdot \left(\sqrt{1 + \frac{2(\gamma\text{-}1)}{\gamma} \cdot \frac{E}{N} \cdot \frac{N_0}{p \pi a_0^2} \cdot q_L \cdot \Delta x_L} - 1\right) (3.3)$$

Lalande [18] discretizes the channel radius evolution, so the leader is composed of several segments. In each segment, the radius and internal electric field change every time step in an iterative methodology (3.4):

$$a_j^2 = a_{j0}^2 + \frac{(\gamma-1) \cdot E_j \cdot \Delta Q_{sc}}{\gamma \cdot \pi \cdot p} \qquad (3.4)$$

where a_j and a_{j0} are the present and previous leader *j*-segment radius, E_j is the *j*-segment internal electric field, and Δx_L is the segment length. Based on a constant particle number, i.e. $N_j \cdot \pi a_j^2 = N_{j0} \cdot \pi a_{j0}^2$ (where N_j is the particle density of the *j*-segment), the reduced electric field is constant at each segment at any time. The evolution of the leader segment internal electric field can be estimated as (3.5):

$$E_{Lj} = \frac{E_{Lj0}}{N_{j0}} N_j \qquad (3.5)$$

where the sub-index 'j_0' in the electric field (E_{j0}) and the particle density (N_{j0}) indicate the variable previous value in the *j*-segment. By knowing the evolution of the internal electric field, it is possible to estimate the leader tip potential (U_{Ltip}) as (3.6):

$$U_{Ltip} = U_0 - \sum_{j=1}^{n} E_{Lj} \cdot \Delta x_{Lj} \qquad (3.6)$$

3.2.   Leader channel model parameter analysis

The leader channel model analysis was done in **Paper II** and **VI** by modifying input parameters in both Rizk's and Lalande's models (Section 3.1) to evaluate their influence on the output variables such as the leader tip potential, the LCR length, the breakdown voltage and the breakdown time.

The analysis was done in comparison with the experimental data reported in [2] of a breakdown event. It consisted of data pairs of the leader tip location and time extracted from a full discharge streak image, as shown in Fig. 4.
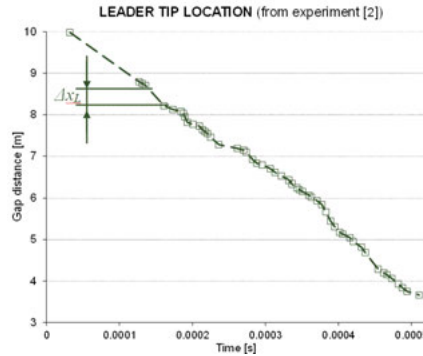

Figure 4. Leader tip location. Experimental data from a discharge streak image [2]

The experimental setup consisted of a 10 m rod-to-plane electrode arrangement in air, tested with positive voltage switching impulses of $U_{cr} = 1.7$ MV and 500/10000 μs waveshape. The tip of the rod was a 10 mm radius cone. The leader tip location was used as the common data input for both models. In the Rizk model the leader length was used directly in (3.1). For the Lalande model, the leader channel was discretized into leader segments. Then, these segment lengths were multiplied by a constant charge per unit length q_L to obtain the charge increments used in (3.4), i.e. $\Delta Q_{SC} = q_L \cdot \Delta x_L$. The input parameters modified for both models are presented in Table 1.

Table 1. *Model parameters modified for comparison*

Model	Parameter	Range	Description
Rizk	E_i	300 – 500 kV/m	Initial leader gradient
Rizk	E_∞	20 – 50 kV/m	Final/ultimate leader gradient
Rizk	x_0	0.5 - 1 m	Space constant
Lalande	E_{SC}	300 - 500 kV/m	LCR potential gradient
Lalande	q_L	20 - 50 μC/m	Electric charge per unit length along the leader channel

In total, 60 cases for the Rizk model and 45 cases for the Lalande model were analysed with the parameter combinations shown in Table 1. Figs. 5 and 6 summarize the results. For the Rizk model (Fig. 5), the results where both $E_i \geq 450$ and $E_\infty \geq 40$kV/m, the final jump condition was achieved after the voltage impulse reached the crest time (500 μs).
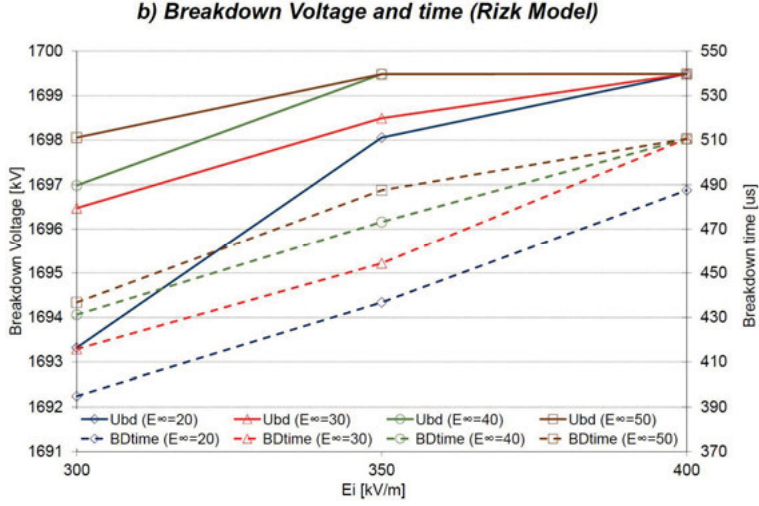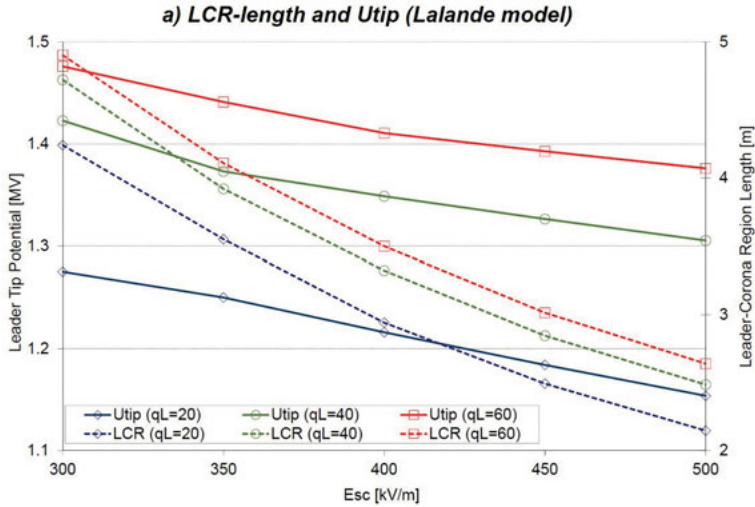

a) LCR length and Utip (Rizk model)
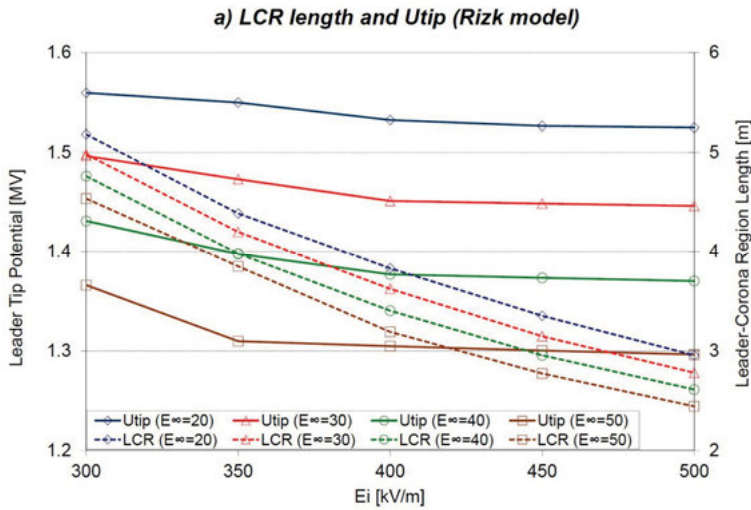
Figure 5. **a)** Leader tip potential (U_{tip}, solid lines) and LCR length (dashed lines) as a function of E_i and E_∞ using the Rizk model at the final jump condition (except cases with both $E_i \geq 450$ and $E_\infty \geq 40$ kV/m. **b)** Breakdown voltage (solid lines) and breakdown time (dashed lines) as a function of E_i and E_∞ using the Rizk model (except the cases with $E_i \geq 400$ kV/m). The value of x_0 (3.1) used for plots a) and b) was x_0=0.75 m.

For the Lalande model (Fig. 6), in the cases where both $E_{SC} \geq 450$ kV/m and $q_L > 50$ µC/m, the final jump condition was achieved after the voltage impulse reached the crest time (500 µs).
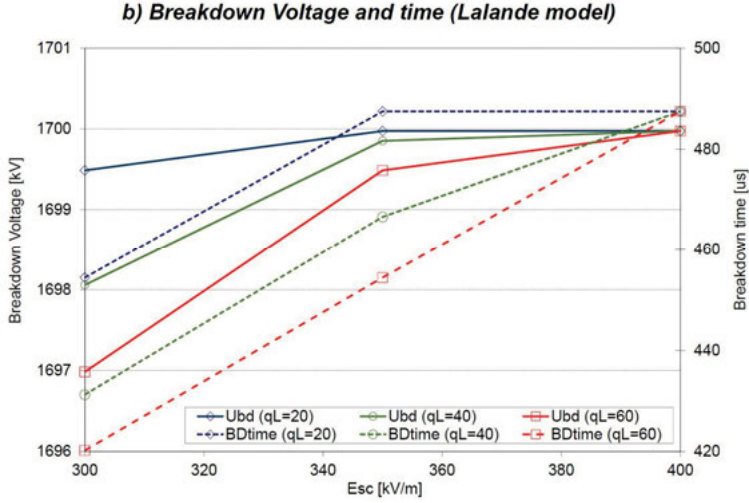
Figure 6. **a)** Leader tip potential (U_{tip}, solid lines) and LCR length (dashed lines) as a function of E_{SC} and q_L using the Lalande model at the final jump condition, except the cases with both $E_{SC} \geq 450$ kV/m and $q_L \geq 50$ µC/m. **b)** Breakdown voltage (solid lines) and breakdown time (dashed lines) as a function of E_{SC} and q_L using the Lalande model (except cases where $E_{SC} > 400$ kV/m)

3.3. Experimental work on leader channel tortuosity and propagation velocity

Paper III reports on experimental work done on leader tortuosity and propagation velocity for laboratory long air gaps. A rod-to-plane electrode arrangement with a gap of 7 and 8 m was tested with positive voltage switching impulses. One of the main interests was to have first-hand electrical and optical records for the full discharge. For the optical records, two still cameras (Cam1 and Cam2) and one fast CCD recording camera were used to acquire images of the full discharge events.

The still camera images were software processed to find the two-dimensional leader path between the rod tip and the ground plane. Then, using projective geometry for each still image from two different points of view, the Cartesian orthogonal three-dimensional location of the channel was found for each discharge. The original and the processed images and the leader path for an 8 m gap test, are presented in Figure 4.
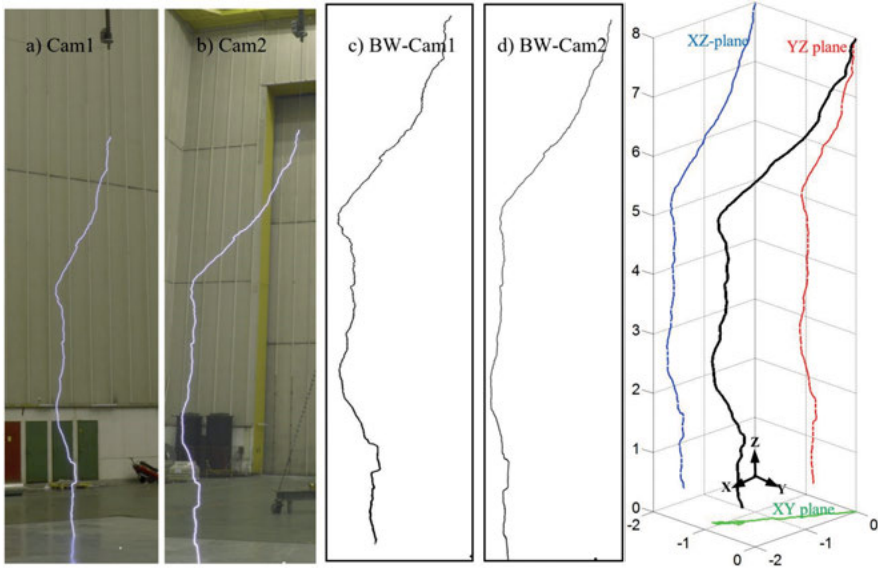
Figure 7. **a, b)** Original still images from two different angles; **c, d)** black and white software processed images of the original photos; **extreme right:** reconstructed leader three-dimensional path and its projections on the Cartesian orthogonal planes.

For the leader propagation velocity estimation, a fast CCD camera (time between frames 2.86 µs) was placed beside Cam1. Fig. 8 shows samples of the frames acquired with the fast CCD camera for the same test as in Fig. 4.
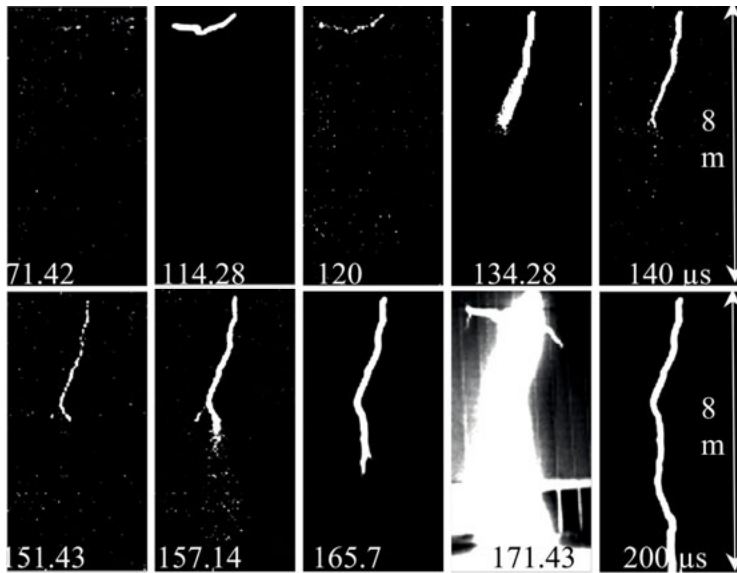

Figure 8. Fast CCD camera frames for an 8 m positive voltage switching impulses. Note the restrike events on the frames labelled t=114.28 and t=134.28 µs and a branching event at t=140 µs.

After the software image processing, it was possible to estimate the changes in the direction of the leader tip on its way to the ground and its propagation velocity from the fast CCD camera records. Following the angle description given by Gu et al. [31] (see Fig. 9), the leader tortuosity can be described with three angles:
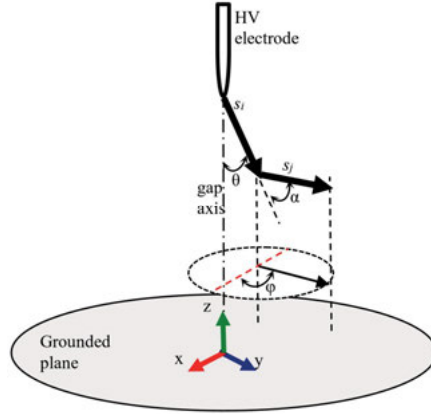

Figure 9. Tortuosity angles proposed by Gu et al. [31]

α – angle between two consecutive leader segments $(0, \pi)$

θ – the leader segment inclination with respect to the gap axis; also known as the polar angle $(0, \pi)$

φ – the leader segment projection on a reference plane (e.g. XY), also known as the azimuthal $(-\pi, \pi)$

From the experimental work, the angles between the leader segments were calculated and their probability density functions estimated. A summary of the functions found for the analysed leader channels is presented in Table 2.

Table 2. *Probability density functions for the tortuosity angles calculated*

Leader Angle	PDF type	Mean	Variance
α – alpha	Log-normal	6.3	34.5
θ – theta (polar)	Log-normal	20.9	437
φ – phi (azimuth)	Non-parametric, normal kernel	(bandwidth 20.3)	

From a combination of the still and fast CCD camera records, it was possible to estimate the propagation velocity of the leader tip. The mean leader velocities were 8.5 and 9.4 cm/µs for the 8 and 7 m gap length respectively. The tortuosity angles and leader velocity are in good agreement of with the findings reported in [31, 36].

4. Methodologies for the full breakdown modelling

One of the main interests of the scientific community working on long air gap breakdown is helping the design of HV equipment insulation by accurately predicting the $U_{50\%}$ for a given electrode arrangement. Through experiments, different electrode configurations have been tested with lightning and switching voltage impulses. Important characteristics were visualized, such as the U-curves found for the $U_{50\%}$, while modifying the time-to-crest for a single electrode geometry [1, 11].

As discussed in Section 3.1 for leader channel models, there are two approaches that can be used for the estimation of the $U_{50\%}$ of a long air gaps tested with positive voltage switching impulses: engineering models and physical models. In the following subsections, some engineering models and methodologies based on physical models are briefly presented as it is an important base for this thesis.

4.1. Methodologies based on engineering models

4.1.1. Lemke model

This model [37] considers the final jump stage of the full discharge and is based on the fact that the total potential difference across the gap is the sum of the voltage drops along the leader channel and the LCR. The gradient in the LCR is assumed constant (E_S) and the variation of the potential along the leader channel would depend on the total gap length (d), and a parameter a_0. This model predicts the $U_{50\%}$ for a given electrode configuration e.g. the rod-plane, the bundle conductor-plane or the bundle conductor-tower, by giving different values to a_0.

4.1.2. Aleksandrov model

In this model [38], a critical charge Q_{cr} formed near the positive HV electrode is a prerequisite for a continuous leader development. Q_{sc} is made of the charge on the electrode at the streamer onset, plus the space charge at the leader inception. This charge relates to the $U_{50\%}$ through the equivalent capacitance of the electrode.

4.1.3. Jones model

Jones model predicts the $U_{50\%}$ of the rod-to-plane and explains the U-shape dependence of the positive voltage switching impulses strength with the impulse time-to-crest. The model indicates that in a gap of length d, with a leader length l_Z, a threshold potential should be surpassed in order to sustain continuous leader propagation. The potential along the channel is considered proportional to its length times the constant gradient [7].

4.1.4. Carrara-Thione model

The model [13] is based on laboratory measurements for the rod-to-plane and conductor-to-plane conductor. It introduces the concept of a critical radius for the HV electrode, above which the streamer and streamer-to-leader transition occur at almost the same voltage. Below critical, the voltage for the streamer inception remains practically constant at the same value of voltage for the electrode with the critical radius. This radius can be determined experimentally for different gap distances and different electrode tip radii.

4.1.5. Hutzler model

This model [33] is based on Jones model from Section 4.1.3 to calculate the temporal development of the leader in a rod-to-plane configuration. It requires a critical field E_c of 31 kV/m for the leader propagation on an equivalent leader radius of 0.3 m. It considers the leader current in terms of the electric field, which is related to the propagation velocity with the constant q_L (Section 3.1). The internal leader gradient is governed by a differential equation that accounts for the time variation of the electric field. It is assumed that the leader propagates in segments and a random angle referenced to the discharge axis is considered for each new segment to include the leader tortuous propagation.

4.1.6. Bazelyan model

For this case [34], the electrostatic energy deposited in the equivalent spark channel capacitance is considered as the upper limit for the energy released in the channel. The equivalent leader capacitance is set to 25 pF/m and the streamer-to-leader transition happens at a minimum voltage between 200 – 300 kV. The leader internal gradient is estimated from an empirical formula as a function of the leader current and life time. Another experimental expression is used to correlate the leader propagation speed with the leader tip potential.

4.1.7. Rizk model

Similar to the previous models, for the rod-to-plane configuration, the positive streamers converge to an ionized stem at the HV electrode. The LCR and

the early leader stem (length s) are represented by a point charge Q_0 located at a distance s_0 from the HV electrode, much shorter than the gap length. The background electric field E_{lc} at the stem tip is given by $E_{lc} = U_{lc}/r_{eq}$, where U_{lc} is the HV electrode voltage and r_{eq} is the stem equivalent radius.

The continuous leader propagation happens when the electric field at the stem tip exceeds a critical level E_{cr}. The final jump (h_{fj}) stage will take place when the leader tip potential is equal to $U_{lc} = E_{SC} \cdot h_{fj}$, where E_{SC} is the constant positive streamer gradient in front of the leader tip [17, 35, 39].

4.2.   Methodologies based on physical models

There has been more interest in the full discharge modelling these last decades, because of the possibility to incorporate more complex elements of the different stages of the discharge within a single methodology. There are different approaches by authors such as Los [40] and Fofana [20, 41]. However, the Lightning Research group at Uppsala University has been particularly interested in methodologies based on the work of Gallimberti [9], like the work of Lalande [18] and Goelian [19]. This is due to their accuracy and the easy implementation for several cases related to long air gaps and lightning attachment as shown by Becerra [21, 22], Arevalo [23, 24] and this dissertation. One element that is common to all of them is the calculation of the electric charge available in the LCR to feed the leader channel as it propagates towards ground. This topic was analysed in **Paper IV** and is presented in Chapter 5.

4.2.1. Lalande-Goelian methodology

This methodology [19] is based on previous works [18, 42]. It consists of four main physical processes:

a)   The Leader Corona Region (LCR), also known as corona region: requires a minimum electric field to sustain further ionization in front of the leader tip.

b)   The leader tip (or head): the charge injected from the LCR produces Joule heating of the cold gas in front, converting the cold diffuse glow at the LCR into a hot channel.

c)   The leader channel: weakly ionized plasma with low internal potential gradient that expands radially

d)   The streamer-leader system: allows the propagation of the whole discharge given that the ionization at the LCR supplies charge and energy to the channel. The latter has an internal low potential drop allowing a potential high enough at the leader tip to sustain discharges further at the LCR.

A schematic representation of the potential distribution for the rod-to-plane electrode arrangement is shown in Fig. 10.
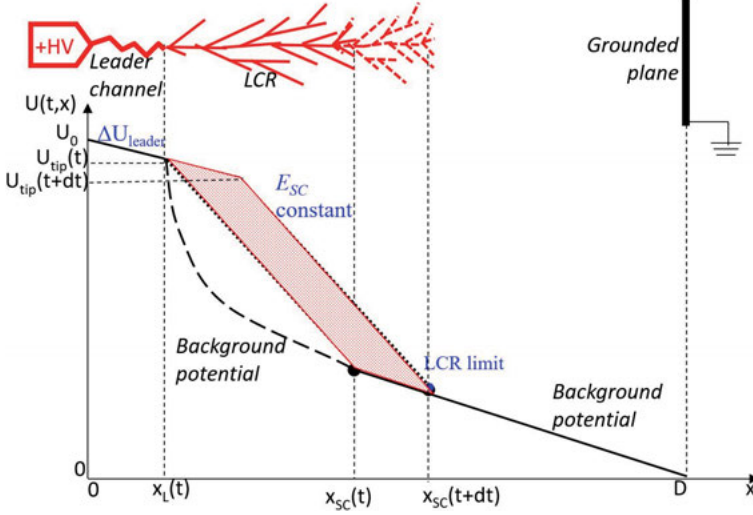

Figure 10. Potential distribution along the discharge axis for a positive discharge. Note the locations of the leader tip (x_L), the LCR limit or streamer front (x_{SC}) and the grounded plane at a distance D.

The methodology's major assumptions are based on the electrostatic representation of the different stages of the discharge, such as the space charge, the potential distribution and gradients. The background potential distribution is solved analytically for hyperbolic electrodes. The streamer inception (Section 2.1) is achieved when the criterion (2.2) is fulfilled. The potential gradient inside the LCR (E_{SC} in Fig. 10) is constant and superimposed over the background potential distribution to find the LCR limit. The amount of charge available in the LCR is proportional to the shaded area in Fig. 10 and a factor K that considers all the streamers in the LCR as lineal distributions of the charge. The amount of LCR charge injected to the leader channel during each simulation step represents an increment in the channel length through the constant q_L, ie. $\Delta x_L = q_L \cdot \Delta Q_{SC}$.

The leader's internal potential during its propagation is calculated following the leader channel model of Lalande (Section 3.1). The breakdown condition is achieved when the LCR limit reaches the reference plane. During the leader progression, if the estimated charge within the LCR becomes negative, the withstand condition has been achieved. A general flow chart of the methodology is presented in Fig. 11.
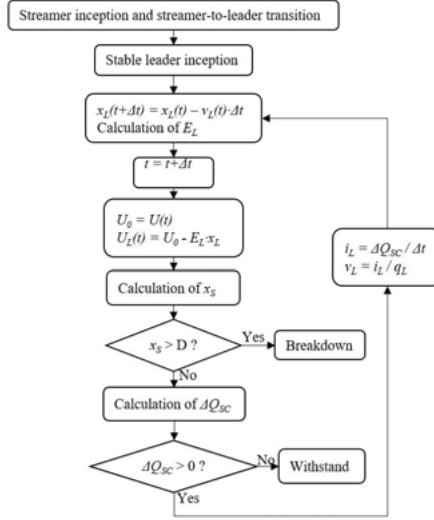
30

Figure 11. Flow chart of the Lalande-Goelian methodology (adapted from [19])

4.2.2. Becerra-Cooray methodology

Based on the Lalande-Goelian methodology, the Becerra-Cooray methodology uses the geometric potential distribution which changes in time and space as the leader propagates, similar to the potential distribution shown in Fig. 10. The methodology has its own approach to evaluate the amount of charge in the LCR (see Section 5.1.3). The electrostatic calculations are done with the help of a FEM solver. Developed for the study of leader inception at grounded structures during the lightning flash event, it is also validated for long air gap experimental data from *Les Renardières* group [2] in [43, 44].

4.2.3. Arevalo methodology

The Arevalo methodology is also based on the Goelian-Lalande methodology, and uses the time-space dependent potential distribution of the discharge gap. It has its own method for calculating the LCR charge (see Section 5.1.4). All of its electrostatic potential calculations are done using a FEM solver. The model includes statistical delays due to streamer inception and tortuosity of the leader channel based on experiments. Its main interest is to determine the $U_{50\%}$ for different inter-electrodic configurations tested with positive voltage switching impulses, in addition to the lightning attachment of grounded structures [45, 46].

4.2.4. New proposed methodology

The new proposed methodology (**Paper V**) is also based on the Goelian-Lalande methodology and makes use of the potential geometric distribution of Fig. 10 to estimate the LCR limit. It combines new features with some elements of the previous methodologies to estimate the $U_{50\%}$ in an up-and-down routine for different inter-electrodic configurations tested with positive voltage switching impulses. Some new features are:

- A statistic time delay time for the dark period between the streamer inception and the streamer-to-leader transition, depending on the electrode sharpness.
- Two new methods for the calculation of the LCR charge proposed in **Paper IV** (see Section 5.2).
- The generation of a random path for the leader channel when propagating based on experimental measurements of long air gap laboratory leaders tested with positive voltage switching impulses (Section 3.3).
- A code-controlled use of the FEM solver for the electrostatic potential calculation, which permits the construction of non-symmetric objects representing the electrodes, the leader channel and the LCR for a long laboratory air gap.

This methodology uses the streamer inception criterion from Meek [27, 28] (Section 2.1), the streamer-to-leader criterion from Gallimberti [9] (Section 2.2) and the Lalande leader channel model (Section 3.1). Fig. 12 presents a general view of the flow diagram for the new proposed methodology.
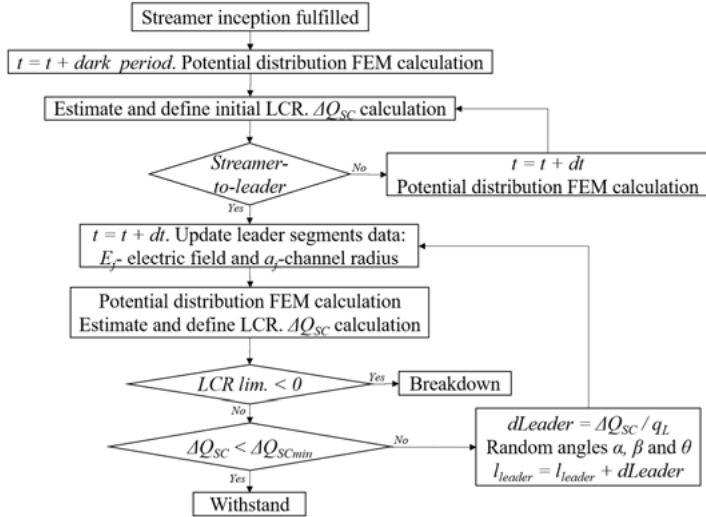

Figure 12. Flow diagram for the methodology proposed in this dissertation for the calculation of breakdown/withstand condition for a full discharge event.

5. Methods for the LCR charge calculation

As mentioned in the previous section, all the analysed methodologies for the estimation of the breakdown in a positive long air gap require a procedure for the calculation of the LCR charge in front of the leader tip as it propagates. Given the complexity of all the physical phenomena occurring in the streamer-leader system, good approximations have been made to explain the physical quantities involved in greater detail [9, 15]. The most common approach to this estimation starts with simplified theoretical models combined with some of the measurable physical variables of the discharge. Most times, these variables exclude the potential or the electric field magnitudes of the leader channel, and are mainly limited to voltage and current measurements and optical records, like those done in **Paper IV**. The next subsections are divided into the preliminary methods available in the literature and two new methods proposed in this work.

5.1. Preliminary methods

5.1.1. Charge Simulation Method

This method was used extensively a few decades ago as the main electric field calculation tool [47, 48]. The method consists of fictitious unknown charges located close to a known potential boundaries (control points), and same-magnitude, opposite-sign image charges equidistant from a symmetry plane in the middle. Castelliani [49] used this technique to analyse the bi-leader discharge, representing the LCR like a series of charge rings. The potential of the control points is assigned following the procedure described in Section 4.2.1 (see Fig. 10). The total charge enclosed in the LCR is calculated by adding the charge of all the rings. Fig. 13 shows a general representation of the LCR built from charge rings and potential points.
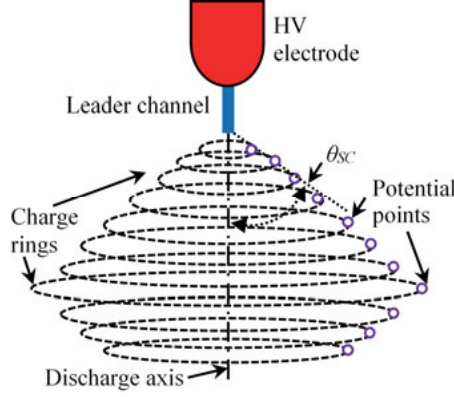
Figure 13. Potential points and charge rings for the CSM representation of the LCR in a rod-to-plane.

5.1.2. Lalande Method

Presented in [18, 19], the LCR limit in this method is determined following the geometric construction for the potential profile described in Section 4.2.1. The LCR charge is calculated considering the streamers as a collection of several parallel charge segments, between the leader tip and the LCR limit. In the rod-to-plane configuration, the amount of charge in the LCR is estimated by finding the area enclosed by the background potential profiles and the superimposed constant potential gradient along the LCR (the shaded region in Fig. 10), multiplied by a factor K that considers the segments' number and geometry.

5.1.3. Becerra-Cooray Method

This method estimates the LCR charge from the difference between the areas enclosed by the geometrical potential distribution of the constant potential gradient in E_{SC}; which is superimposed over the background potential in front of the leader tip at two successive moments of the leader progression [21] (similar to the shaded region in Fig. 10). This area is then multiplied by a constant K_Q, estimated from the CSM (Section 5.1.2) for different geometries. In more recent work of Becerra [50], the LCR streamer charge is estimated by solving the Poisson inverse problem by optimization in the streamer region

5.1.4. Arevalo Method

In this method [24], the electrostatic potential distribution in the simulation domain is calculated with a FEM solver. The output is then compared following the procedure described in Section 4.2.1, to determine the electric field lines that fulfil the condition of the constant potential gradient E_{SC} to sustain

34

streamer discharges in the LCR. Then, the volume that fulfils the condition is divided into *n*-layers. The electric charge in each layer is equal to the electric flux through a Gaussian surface that encloses the layer (5.1). Then, the total electric charge inside the LCR results from adding the individual charges dQ_j found for each layer (5.2):

$$dQ_j = \oint_{S_j} \varepsilon_0 \vec{E} \cdot \vec{ds} \quad (5.1)$$

$$Q_{SC} = \sum_{j=1}^{j=n} dQ_j \quad (5.2)$$

Fig. 14 shows a schematic representation of the LCR calculation elements used in this method.
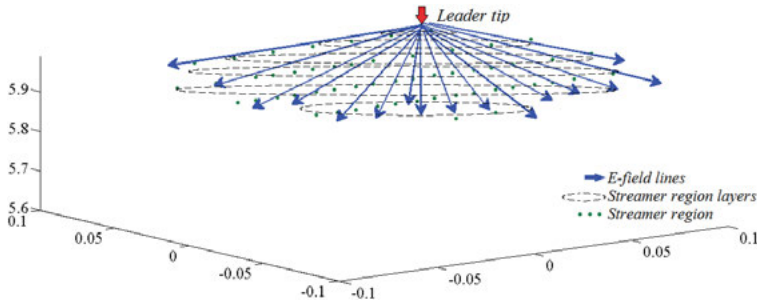

Figure 14. LCR representation used for the calculation of the total LCR charge with the Arevalo method (adapted from [24])

5.2.   New proposed methods

Based on electrostatic principles like the Gaussian electric flux integral and the capacitance matrix, two new methods were proposed for the calculation of the LCR charge. Since the FEM solver can be easily controlled by an external program in an iterative loop, the geometry of the configuration and the boundary conditions can be modified continuously to implement either of the following methods for the LCR charge calculation in the new proposed methodology (Section 4.2.4). In both cases, the LCR is represented as a group of ring pseudo-electrodes, with potentials assigned following the procedure described in Section 4.2.1. This means that both methods can be implemented from the same electrostatic potential solution. Fig.15 presents an example of the geometry simulated in FEM for a rod-to-plane electrode arrangement.
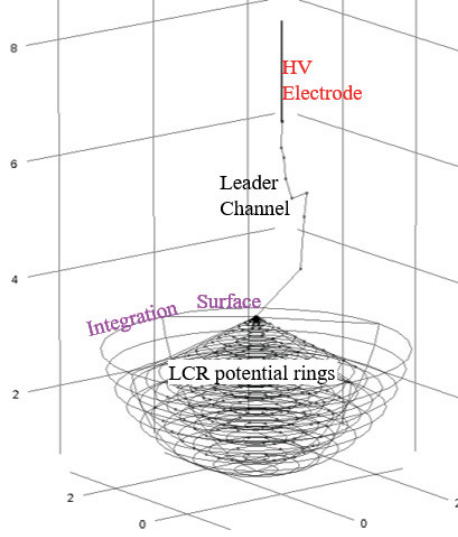
Figure 15. Elements used for the representation of the full discharge in long labora-
tory air gaps. Note the LCR potential rings surrounded by the Gaussian integration
surface.

Previously, Masloswki [51] used the Gaussian integration for estimating
lightning channel corona and Ortega [52] used it for the study of the corona
onset in long air gaps. In the Single Surface Integral (SSI) method, all the
pseudo-electrodes in the LCR are surrounded by a unique closed surface *S*,
and the electrical flux through this surface was evaluated to obtain the amount
of net charge inside (5.3):

$$Q_{SC\ total} = \oint_S \ \varepsilon_0 \vec{E} \cdot \vec{ds} \qquad (5.3)$$

where $Q_{SC\ total}$ was the net charge enclosed by the Gaussian surface *S*, ε_0
was the vacuum permittivity and *ds* was the infinitesimal differential area nor-
mal to the Gaussian surface *S*.

For the Capacitance Matrix Method (CMM), the capacitance matrix ele-
ments (C_{ij}) were calculated for all the electrodes and pseudo-electrodes with
potential U_i by integrating the electrical energy density for each *i*-electrode
over the whole simulation domain Ω (5.4).

$$C_{ii} = \frac{2}{U_i^2} \oint_\Omega \ W_E \cdot d\Omega \qquad (5.4)$$

Then, the lineal system with *i*-equations was solved for all known *i*-poten-
tials, so all charges Q_i can be estimated (5.5).

$$\begin{bmatrix} Q_1 \\ \vdots \\ Q_i \end{bmatrix} = \begin{bmatrix} C_{11} & \cdots & C_{1i} \\ \vdots & \ddots & \vdots \\ C_{i1} & \cdots & C_{ii} \end{bmatrix} \cdot \begin{bmatrix} U_1 \\ \vdots \\ U_i \end{bmatrix} \qquad (5.5)$$

Thus, the total charge in the LCR can be estimated by adding all the charges from all the ring k-pseudo-electrodes (5.6):

$$Q_{SC\,total} = \sum_{j=1}^{j=k} Q_j \qquad (5.6)$$

In **Paper IV**, the methods of CSM, Becerra-Cooray, Lalande, SSI and CMM were compared to experimental data for streamer inception in a rod-to-plane configuration from *Les Renardières* group [2]. A summary of the results found in **Paper IV** is presented in Fig. 16.
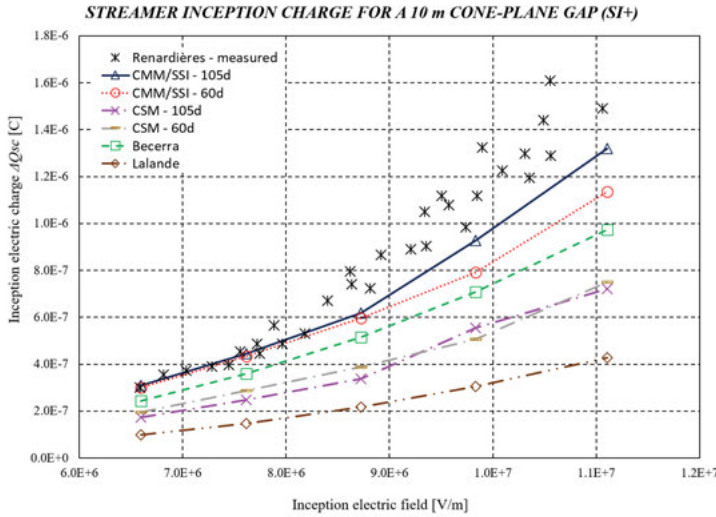

Figure 16. Results from the comparison between different methods for the calculation of the LCR charge at the moment of streamer inception.

In the case of the CSM, the simulation domain only included the electrode, the LCR potential rings and their images below to represent the grounded reference plane. On all the other cases, the simulation domain consisted of a grounded box with the dimensions of the HV laboratory. This slight difference may affect the results obtained for CSM in comparison with the other methods. For the Lalande model, the number of streamer segments and geometric parameters were set in a specific way. Different values of these parameters might give results closer to the measured values.

The effect of modifying the cone semiangle θ_{SC} (see Fig. 13) on the amount of charge in the LCR was studied by Becerra [50] and Ortéga [52]. As it can be seen in Fig. 16, the better accuracy between the simulated values and the measured ones, was found for the larger θ_{SC} in the CMM and SSI, in accordance with the conclusions of Becerra [50], where the charge estimations become almost angle independent for larger values of θ_{SC}.

6. Results from the new methodology

The new proposed methodology was used for the calculation of $U_{50\%}$ in common electrode configurations and non-symmetric geometries including protrusions. The experimental values reported by Wu et al [53] were used as the main reference for comparison. In Wu's work different electrode configurations like rod-to-plane and sphere-to-plane (with and without protrusions) are analysed and their $U_{50\%}$ calculated from laboratory measurements. The protrusions consisted of small rods of 5 mm radius and 10 or 50 mm length located on the sphere surface pointing towards the grounded plane (under protrusion –UP–) or perpendicular to the main gap axis, at the sphere equatorial plane (side protrusion –SP–). All the electrode configurations were tested with positive voltage switching impulses 275/2500 µs.

In the **Paper V**, the $U_{50\%}$ was calculated using the up-and-down method [54, 55] for each electrode configuration. In the 50 simulated events, the breakdown or withstand condition was found for each event. Due to the simplicity of the code controlling the FEM solver, the CMM (Section 5.2) was used for the calculation of the LCR charge in all cases. The main physical parameters used throughout the simulations were: a) the constant gradient in the LCR set at 450 kV/m, and b) the constant charge per unit length q_L was set to 36 µC/m considering the conclusions of Gallimberti for the effect of humidity (relative humidity of 50% at the testing site) and impulse wavefront [2, 9].

The potential excitation for the HV electrode was set as suggested by Fofana [20] like a double exponential function of time, with three input parameters: crest voltage U_{cr}, time to crest T_{cr} and T_2 time to half-value. The following subsections present a summary of the results obtained for each configuration.

6.1. Rod-to-plane

A general view of the tested setup and the geometry simulated are presented in Fig. 17.
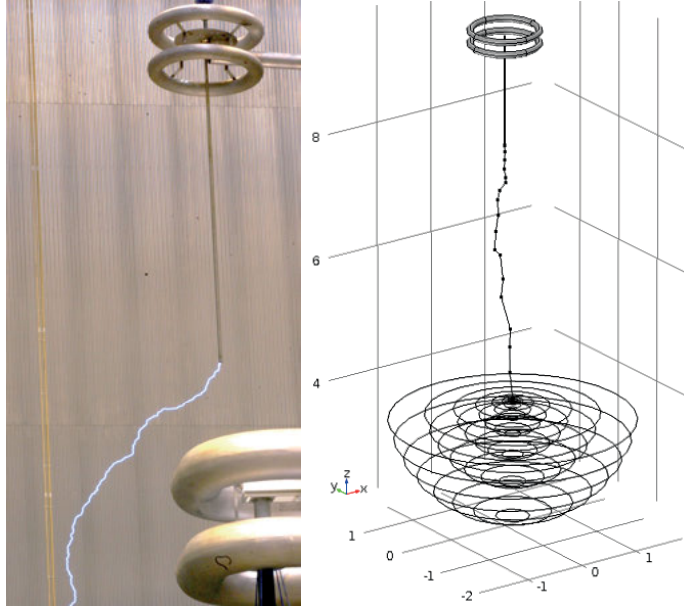

Figure 17. Tested rod-to-plane configuration and its simulated representation (photo courtesy PSGS HVDC ABB AB).

The electrode was an aluminium rod with a radius of 15 mm and a length of 3 m. Three gap distances were analysed and the obtained results are included in Table 3. The values marked (*) were estimated using the formula proposed by Paris [11] for the rod-plane configuration, $U_{50\%} = 500 \cdot d^{0.6}$.

Table 3. *Experimental values and simulation results for rod-to-plane electrode configuration*

Test	Gap [m]	$U_{50\%}$ measured [kV]	$U_{50\%}$ calculated [kV]	Error %
1	6	1447	1567	-8.3%
2	8	1741*	1846	-5.0%
3	10	1990*	1994	-0.2%

There was a good agreement between the simulation and the measured values for this configuration, and the accuracy was better for the larger gap distances.

6.2. Sphere-to-plane

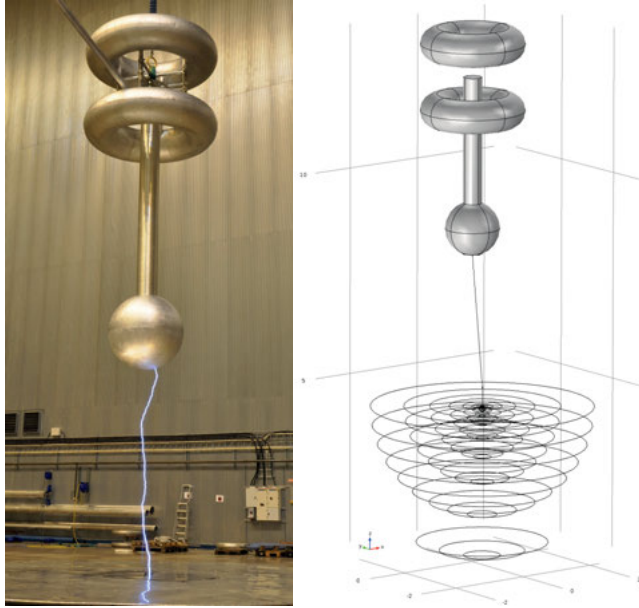The tested setup and the geometry simulated are shown in Fig. 18.

Figure 18. Sphere-to-plane electrode arrangement and its simulated representation (photo courtesy PSGS HVDC ABB AB).

Aluminium spheres with different diameters were attached to a tube with a length of 450 mm terminating in two toroids for electric field relief at the connection point to the impulse generator. Three diameters and three gap distances were analyzed and the obtained results are included in Table 4.

Table 4. *Experimental values and simulation results for sphere-to-plane electrode configuration*

Test	Gap [m]	Sphere radius [m]	$U_{50\%}$ measured [kV]	$U_{50\%}$ calculated [kV]	Error %
1	6	0.65	2227	2199	1.2%
2	8	0.65	2331	2288	1.8%
3	4	0.8	2411	2308	1.2%

For this configuration the average error was the lowest for all simulated electrode configurations. In some cases, the simulated tests terminated in withstand condition and did not reach the streamer inception condition. In the other cases, the breakdown happened a few steps after the streamer-to-leader transition, acting almost as a breakdown caused only by streamer discharge.

6.3. Sphere-to-plane under protrusion

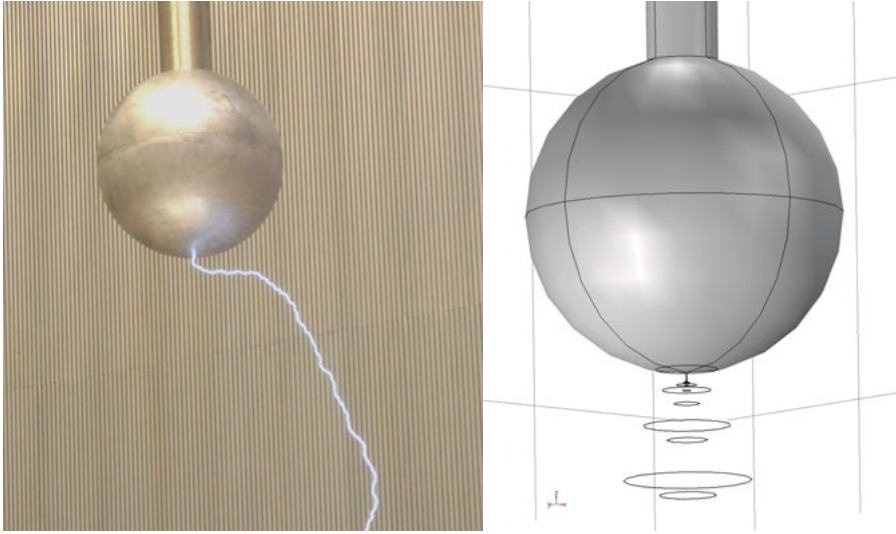A general view of the simulated geometry and the tested setup are presented in Fig. 19.

Figure 19. Setup sphere-to-plane with protrusion under and its equivalent simulated model (photo courtesy PSGS HVDC ABB AB).

Small rods with a radius of 5 mm and a length of 10 and 50 mm were located on the closest point of the sphere to the ground, on the sphere axis perpendicular to the grounded plane. Three diameters and gap distances were analysed and the obtained results are included in Table 5.

Table 5. *Experimental values and simulation results for sphere-to-plane under protrusion electrode configuration*

Test	Gap [m]	Sphere radius [m]	Protrusion length [mm]	$U_{50\%}$ measured [kV]	$U_{50\%}$ calculated [kV]	Error %
1	8	0.65	50	1861	1662	10.7%
2	4	0.8	50	1248	1011	19.0%
3	6	0.8	50	1561	1487	4.7%
4	8	0.8	50	1812	1696	6.4%
5	4	1	50	1295	1024	20.9%
6	8	0.65	10	2153	1776	17.5%
7	4	0.8	10	1484	1018	31.4%
8	6	0.8	10	1955	1368	30.0%
9	8	0.8	10	2202	1792	18.6%
10	4	1	10	1536	918	40.2%

This configuration had larger errors than to the other simulated geometries with and without protrusions, especially in the cases with the larger electrode radius, shorter gap distances and shorter protrusion length.

The representation of the used LCR seems to be more accurate if the inhomogeneity of the electric field on the HV electrode is more accentuated. It can be seen in Table 5 how the larger errors were found for the shorter protrusions on larger spheres at shorter gaps, i.e. when the electric field stress on the protrusion tip is less intense.

6.4. Sphere-to-plane side protrusion

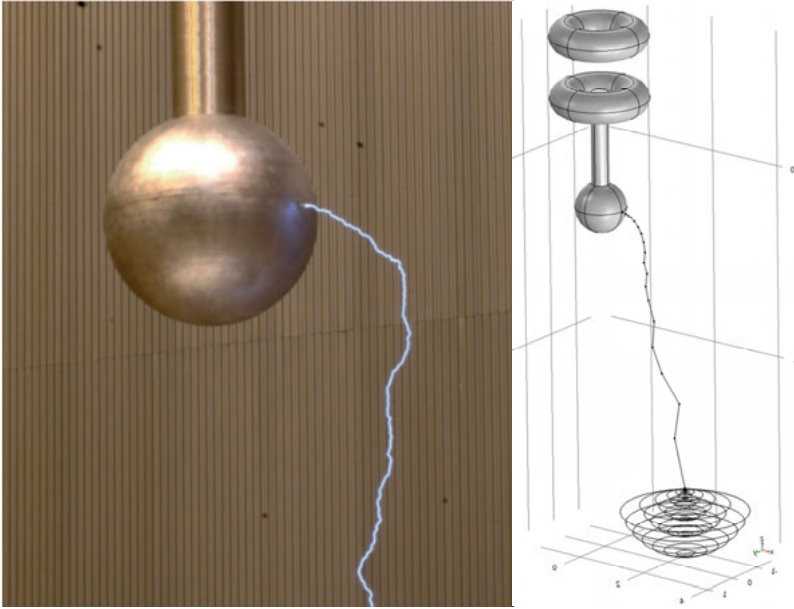A general view of the geometry simulated and the tested setup are presented in Fig. 20.

Figure 20. Tested sphere-to-plane with side protrusion and its equivalent simulated model (photo courtesy PSGS HVDC ABB AB).

Small rods with a radius of 5 mm and a length of 10 and 50 mm were located on a point on the equatorial plane of the sphere, parallel to the grounded plane. Three radius and gap distances were analysed and the obtained results are included in Table 6.

Table 6. *Experimental values and simulation results for sphere-to-plane side protrusion electrode configuration*

Test	Gap [m]	Sphere radius [m]	Protrusion length [m]	$U_{50\%}$ measured [kV]	$U_{50\%}$ calculated [kV]	Error %
1	8	0.65	50	1856	1682	9.4%
2	4	0.8	50	1432	1479	-3.3%
3	6	0.8	50	1657	1552	-6.3%
4	4	0.8	50	1941	1553	6.3%
5	4	1	50	1514	1512	0.1%
6	8	0.65	10	2059	1716	16.6%
7	4	0.8	10	1602	1391	13.1%
8	6	0.8	10	1900	1606	15.5%
9	8	0.8	10	2103	1673	20.4%
10	4	1	10	1659	1326	20.1%

In this configuration there was a better agreement with the measured values for the 50 mm protrusion. Similar to the results found in Section 6.3, it can be seen in Table 6 that the configurations where the sphere radius was larger, the protrusion length shorter and the gap distance shorter, produced larger errors compared to the measured values. This fact might be attributed to the accuracy of the representation of the LCR if the inhomogeneity of the electric field caused by protrusions at the HV electrode less more accentuated.

7. Conclusions

7.1. Leader channel models

Common elements found among the analysed leader models are the constant potential gradient E_{SC} in the LCR to sustain the streamer discharges and the constant charge per unit length along the leader channel q_L. The latter is also related the leader propagation velocity.

Engineering and physical leader channel models are based on common basic elements of the discharge process, such as the streamer inception, the leader inception and progression, the leader channel and the LCR properties. In both types of models, several simplifications and assumptions must be done to make the best use of the model. The discretization of the leader model of Gallimberti [9] done by Lalande [18, 19] simplifies the sequential solution in different simulation methodologies.

The potential gradient required to sustain streamer discharges had a strong influence on the analysed leader models. This basic parameter (E_{SC} in the Lalande model and E_i in the Rizk model) affected the LCR extension in front of the leader tip in both models.

The variation of the models' input parameters permits identifying the effects of the assumptions when modeling leaders. In the Rizk model the reduction of the E_∞ parameter made it possible to elongate the LCR limit further. A larger LCR makes it possible to achieve faster breakdown times at lower breakdown voltages.

In the Lalande model, the q_L affected the leader tip potential, in a way that the length of the LCR that surpassed the threshold of the constant average gradient E_{SC} was larger or shorter. Similar to the Rizk model, a leader channel with a higher electric potential (a higher q_L) will extend the LCR further, achieving the breakdown stage in shorter times and at lower voltages.

7.2. Experimental work on leader channels

Regarding the leader propagation, the use of higher crest voltage values compared to the expected $U_{50\%}$ (overvoltage), increased the average measured leader velocity. However, a detailed variation of the leader velocity as a function of the percentage of overvoltage for an experimental setup similar to the one used was not available in the literature for comparison.

Image processing is still a powerful experimental tool in the study of electrical discharges. The combination of fast and still images permitted determining the leader velocity when propagating in a three-dimensional space. This method can be extended to analyse other discharge mechanisms. In addition, the use of digital records facilitated the data post-processing from the software point of view.

7.3. New proposed methodology

A common element between the different methodologies in the calculation of the LCR charge, also included in the new proposed, is the assumption of a constant potential gradient E_{SC} in the LCR. Two new methodologies, the Single Surface Integral (SSI) and the Capacitance Matrix Method (CMM), were proposed based on the electrostatic potential distribution obtained when representing the LCR as a cluster of ring pseudo-electrodes.

All the methodologies mentioned for the LCR charge estimation include geometrical constants that might eventually influence the result. This effect was seen while assigning the location for the potential rings and fictitious charges in the CSM and the semiangle θ_{SC} for the ring pseudo-electrodes in SSI and CMM.

As the main features of the new proposed simulation methodology, it is worth mentioning that it permitted the inclusion of non-symmetrical elements in three-dimensional geometries and used the SSI and CMM methods for calculating the amount of electric charge in the LCR as the leader propagates. The representation of the used LCR is more accurate if the inhomogeneity of the electric field on the HV electrode is more accentuated. This fact can be observed when comparing the results obtained for shorter protrusions on larger spheres at shorter gaps, for the sphere-under/side protrusion configurations.

The methodology proposed is a continuation of the preliminary work of various authors, who often had common elements in their methodologies. Once there is a good understanding of the phenomena involved, the simulation

methodologies can be analysed as building blocks. In the new proposed methodology, some of the identified blocks are interchangeable, like the calculation of the LCR charge (Section 5.2).

The use of a FEM solver permitted including more elements to the representation of the discharge. The FEM solver was commanded through an external linked code, where a new complete geometry was built for each stage of the discharge, which was then solved. Then, the results were interpreted in a continuous feedback to the main code.

8. Future work

More complex non-symmetric electrode configurations are present in the daily tasks of scientists and engineers designing high voltage equipment. As a first approach, the work in this dissertation only included two of the many possible non-symmetrical configurations found in almost all equipment related to the transmission and distribution of electrical energy. Further analysis using the proposed methodology can be done for different configurations in real cases, including standing insulating structures, hanging cables, etc. A common configuration for which previously published experimental data is available, is the electrode geometry where a sharp element is connected to the grounded structure from which a negative discharge might initiate. It would be an easy task to analyse this matter using the new proposed methodology.

The homogeneity of the electric field at the high voltage electrode has a strong influence on the accuracy of the estimated $U_{50\%}$. Additional work on the representation of the LCR at and after the streamer-to-leader transition should be done, focusing on the region near the surface of large radius electrodes. As was done in **Papers I** and **II**, the sensitivity of the output results based on physical input constants used throughout the new proposed methodology would be significant for future applications.

The new methodology was implemented with simple coding connecting two powerful software tools, one for the data storage and processing, and another for the solution of the FEM geometries that change continuously during the sequential execution of the code. In this form, the calculation times increased to a few days in a small workstation computer for each electrode configuration. The serial execution of the tasks was a first approach to solving the methodology, but it can be further improved if possibility to operate the software tools in parallel is fully exploited. This would make better use of the computational resources and reduce the total calculation time.

9. Summary of papers

Paper I
Leader channel models for long air positive electrical discharges
In this paper, a general review of the available leader channel models proposed for the positive long air gap electrical discharge was done. Common underlying assumptions were found in most of the models analyzed. The comparison with the experimental data revealed that the results obtained from the models were a good representation of the physical situation.
This paper was published in the *Journal of Electrostatics*

Paper II
Parameter variation in leader channel models used in long air gap discharge simulation
In this work, engineering and physical leader models were compared against experimental data recorded for a rod-to-plane electrode arrangement tested with switching voltage impulses. The analysis showed that the leader channel evolution depends strongly on the potential gradient assumed to sustain streamers.
This paper was published in the *Electric Power Systems Research* journal

Paper III
Experimental study of Leader Tortuosity and Velocity in Long Rod-plane Air Discharges
This paper deals with experimental results obtained while testing a long rod-plane air gap with positive switching voltage impulses to study the velocity and tortuous progression of the leader discharge.
This paper was published in the *IEEE Trans. on Dielectrics and Electrical Insulation*

Paper IV
Methodologies for the charge estimation in the leader corona region used in modeling long air gaps under positive voltage impulses
In this paper, departing from the use of a finite element method solver to determine the electric potential distribution, two new methodologies to quantify the amount of charge produced in the leader-corona region were presented and compared with other ones available in the literature.

This paper was included in the *Proc. of the 33rd International Conference on Lightning Protection ICLP 2016.*

Paper V
Numerical modeling of long air laboratory gaps tested with positive switching impulses

In this manuscript, the results obtained using a new version of a simulation methodology for modelling long air gaps were presented. This methodology included new elements like the three-dimensional leader tortuosity from experimental measurements and two new methods for the leader-corona charge estimation. Results from the simulation were compared with experimental records and a good agreement is found between them.

This manuscript was submitted to the *IEEE Trans. on Dielectrics and Electrical Insulation*

10.   Svensk sammanfattning

Denna avhandling handlar om forskning på numerisk modellering av elektriska urladdningar över långa luftgap samt långa spänningsstötar. Den börjar med en förberedande analys av arbete som utförts av ett flertal forskare under de senaste decennierna och analyserar sedan olika metoder för modellering av alla steg i en fullständig urladdning. Relationerna mellan dessa modeller identifieras, liksom effekten på resultatet när viktiga parametrar ändras.

I den allmänna beskrivning av fenomenet ingår tre huvuddelar: streamer starten, streamer till leader övergång och stabil leader utbredning. Dessa element är närvarande i många av de modeller som analyserats och de viktigaste skillnaderna mellan dem är de antaganden och förenklingar som gjorts av varje forskare vid en viss punkt i metodutvecklingen. Gemensamma element som förenklar de analyserade modellerna är de fysiska konstanter i de olika urladdningsmekanismer som finns i en fullständig stöt. Dessa konstanter är potentialgradienten i leader-corona regionen för att upprätthålla leader-förökning, elektrisk laddning per längdenhet i leaderkanalen beroende på atmosfäriska förhållanden och spänningsstötens vågform, och leader-utbrednings-hastigheten, nära besläktad med urladdningsströmmen.

Avhandlingen innehåller resultaten av laborativt arbete med leader mekanismen, men även mätning och analysering av elektriska och optiska signaler. Genom att rekonstruera den tredimensionella leader utbredningen för en stav-till-plan konfiguration var det möjligt att studera den slumpmässigt slingrande bana som följs av leadern när den utbreder sig.

En viktig del i urladdningsmodellen är representationen av leader-corona regionen framför leaderspetsen när den utbreder sig mot den jordade elektroden. Två nya metoder förslås för beräkningen av nettoladdningen som finns i leader-corona regionen, utgående från den elektrostatiska potentialfördelning som erhållits från beräkningsmjukvara baserad på den finita elementmetoden. Detta möjliggjorde införlivandet av flera element som bättre representerar olika delar av urladdingars simuleringen.

I den sista delen av avhandlingen har alla de analyserade elementen, och de nya föreslagna, använts i en ny metod för modellering av elektriska urladdningar i långa luftgap. Denna metod jämfördes med experimentell data. Det fanns en god överensstämmelse mellan simuleringsresultaten och de experimentellt uppmätta mätvärdena.

11.   Resumen en español

Esta tesis trata la modelación numérica de descargas eléctricas en aire para distancias largas en laboratorio, probadas con impulsos positivos tipo maniobra. La tesis inicia con el trabajo preliminar de varios científicos durante las últimas décadas, y luego analiza los diferentes enfoques para modelar todas las etapas de una descarga completa. Las relaciones entre estos modelos fueron identificadas, así como el efecto sobre el resultado final con la modificación de algunos parámetros de entrada importantes.

La descarga eléctrica en distancias largas se puede resumir en tres elementos principales: el inicio de streamer, la transición streamer-leader y la propagación estable del leader. Estos elementos están presentes en la mayoría de los modelos analizados y las principales diferencias entre ellos son los supuestos y simplificaciones realizadas por cada autor. Los elementos comunes que simplifican los modelos analizados son las constantes físicas de los diferentes mecanismos de descarga. Estas constantes son el gradiente de potencial en la región leader-corona para mantener la propagación del leader, la carga por unidad de longitud a lo largo del canal de leader, que depende de las condiciones atmosféricas y la forma de onda de impulso de voltaje, y la velocidad de propagación leader, estrechamente relacionada con la descarga corriente.

Esta tesis incluye los resultados del trabajo de laboratorio en descargas tipo leader en laboratorio, medición y análisis de los registros eléctricos y ópticos. La reconstrucción de la propagación tridimensional del leader para la configuración de punta-plano, permitió estudiar el camino tortuoso aleatorio seguido por el leader a medida que se propaga.

Un elemento importante incluido en el modelo es la representación de la región leader-corona en frente de la punta del leader a medida que avanza hacia el electrodo de tierra. Para el cálculo de la carga neta disponible en la región leader-corona, se propusieron dos nuevas metodologías basadas en la distribución potencial electrostático obtenida con un programa de cálculo basado en el método de elementos finitos. Esto permitió la inclusión de más elementos que representen partes de la descarga durante la simulación.

En la parte final, todos los elementos analizados y los nuevos propuestos se incluyeron en una nueva metodología para el modelación numérica de descargas eléctricas en aire para distancias largas. Esta metodología se comparó con los datos experimentales y se obtuvo buena concordancia.

12.   Acknowledgements

To my primarii lapidis, the cause and the effect, my alpha and omega, my friend, my partner, the mother of my son David, my beautiful wife Pilar. I still cannot imagine how this Ph.D. would have been completed without you. All the good things you have done for me during these years are invaluable. Gracias totales mi amor!

References

[1]   Les Renardières Group, "Research on Long Air Gap Discharges at Les Renardières," Electra, Vol. 23, pp. 53–157, 1972.

[2]   Les Renardières Group, "Research on Long Air Gap Discharges at Les Renardières - 1973 results -," Electra, Vol. 35, pp. 49–156, 1974.

[3]   Les Renardières Group, "Positive discharges in long air gaps at Les Renardieres: 1975 results and conclusions," Electra, Vol. 53, pp. 31–153, 1977.

[4]   R. T. Waters and R. E. Jones, "The Impulse Breakdown Voltage and Time-Lag Characteristics of Long Gaps in Air. I. The Positive Discharge," Philos. Trans. R. Soc. London. Ser. A, Math. Phys. Sci., Vol. 256, No. 1069, pp. 185–212, 1964.

[5]   R. T. Waters, "Breakdown in nonuniform fields," IEE Proc. A Phys. Sci. Meas. Instrumentation, Manag. Educ. Rev., Vol. 128, No. 4, pp. 319–325, 1981.

[6]   G. Baldo, I. Gallimberti, H. Garcia, B. Hutzler, J. Jouarie, and M. Simon, "Breakdown Phenomena of Long Gaps Under Switching Impulse Conditions. Influence of Distance and Voltage Level," IEEE Trans. Power Appar. Syst., Vol. 94, No. 4, pp. 1131–1140, 1975.

[7]   B. Jones and R. Waters, "Air insulation at large spacings," Proc. Inst. Electr. Eng., Vol. 125, No. 11, pp. 1152–1176, 1978.

[8]   W. Büsch, "Air humidity: an important factor for UHV design," IEEE Trans. Power Appar. Syst., Vol. PAS-97, No. 6, pp. 2086–2093, 1978.

[9]   I. Gallimberti, "The mechanism of the long spark formation," Le J. Phys. Colloq., Vol. 40, No. C7, pp. C7–193–C7–250, 1979.

[10]   G. Aleksandrov, "Mechanism of corona-to-spark transition in long air gaps," Sov. PHYSICS-TECHNICAL Phys., Vol. 10, No. 7, pp. 948–951, 1966.

[11]   L. Paris, "Influence of Air Gap Characteristics on Line-to-Ground Switching Surge Strength," IEEE Trans. Power Appar. Syst., Vol. PAS-86, No. 8, pp. 936–947, 1967.

[12]   L. Paris and R. Cortina, "Switching and lightning impulse discharge characteristics of large air gaps and long insulator strings," IEEE Trans. Power Appar. Syst., Vol. 87, No. 4, pp. 947–957, 1968.

[13]   G. Carrara and L. Thione, "Switching surge strength of large air gaps: A physical approach," IEEE Trans. Power Appar. Syst., Vol. 95, No. 2, pp. 512–524, 1976.

[14]   P. Domens, A. Gibert, J. Dupuy, and B. Hutzler, "Propagation of the positive streamer-leader system in a 16.7 m rod-plane gap," J. Phys. D. Appl. Phys., Vol. 24, No. 10, pp. 1748–1757, 1991.

[15]   E. Bazelyan and Y. Raizer, Spark Discharge. 1997.

[16]   R. T. Waters, "Electric gradient in the leader channel of the long spark," 1974.

[17]   F. Rizk, "A model for switching impulse leader inception and breakdown of long air-gaps," IEEE Trans. Power Deliv., Vol. 4, No. 1, pp. 596–606, 1989.

[18]   P. Lalande, "Etude des conditions de foudroiement d'une structure au sol"(doctoral dissertation), Universite de Paris XI ORSAY, 1996.

[19]   N. Goelian, P. Lalande, A. Bondiou-Clergerie, G. L. Bacchiega, A. Gazzani, and I. Gallimberti, "A simplified model for the simulation of positive-spark development in long air gaps," J. Phys. D. Appl. Phys., Vol. 30, No. 17, pp. 2441–2452, 1997.

[20]   I. Fofana and a. Beroual, "A model for long air gap discharge using an equivalent electrical network," IEEE Trans. Dielectr. Electr. Insul., Vol. 3, No. 2, pp. 273–282, Apr. 1996.

[21]   M. Becerra and V. Cooray, "A simplified physical model to determine the lightning upward connecting leader inception," IEEE Trans. Power Deliv., Vol. 21, No. 2, pp. 897–908, 2006.

[22]   M. Becerra, "On The Attachment of Lightning Flashes to Grounded Structures"(doctoral dissertation), Digital Comprehensive Summaries of Uppsala Dissertations from the Faculty of Science and Technology, Acta Universitatis Upsaliensis, 2008.

[23]   L. Arevalo, "Numerical Simulations of Long Spark and Lightning Attachment"(doctoral dissertation), Digital Comprehensive Summaries of Uppsala Dissertations from the Faculty of Science and Technology, Acta Universitatis Upsaliensis, 2011.

[24]   L. Arevalo, D. Wu, and B. Jacobson, "A consistent approach to estimate the breakdown voltage of high voltage electrodes under positive switching impulses," J. Appl. Phys., Vol. 114, No. 8, p. 083301, 2013.

[25]   "COMSOL multiphysics user guide (Version 5.1)," COMSOL, AB, 2015.

[26]   I. Gallimberti, G. Bacchiega, A. Bondiou-clergerie, and P. Lalande, "Fundamental processes in long air gap discharges," Comptes Rendus Phys., Vol. 3, pp. 1335–1359, 2002.

[27]   L. B. Loeb and J. M. Meek, "The mechanism of spark discharge in air at atmospheric pressure. II," J. Appl. Phys., Vol. 11, No. 7, pp. 459–474, 1940.

[28]   L. B. Loeb and J. M. Meek, "The mechanism of spark discharge in air at atmospheric pressure. I," J. Appl. Phys., Vol. 11, No. 6, pp. 438–447, 1940.

[29]   R. Morrow and J. Lowke, "Streamer propagation in air," J. Phys. D. Appl. Phys., Vol. 30, No. 4, pp. 614–627, 1997.

[30]   Y. P. Raizer, Gas discharge physics. 1991.

[31]   S. Gu, W. Chen, J. Chen, H. He, and G. Qian, "Observation of the streamer–leader propagation processes of long air-gap positive discharges," IEEE Trans. Plasma Sci., Vol. 38, No. 2, pp. 214–217, 2010.

[32]   O. Diaz, P. Hettiarachchi, M. Rahman, S. Vayanganie, and V. Cooray, "Experimental study of Leader Tortousity and Velocity in Long Rod-plane Air Discharges," IEEE Trans. Dielectr. Electr. Insul., Vol. 23, No. 2, pp. 806–812, 2016.

[33]   B. Hutzler and D. Hutzler-Barre, "Leader propagation model for predetermination of switching surge flashover voltage of large air gaps," IEEE Trans. Power Appar., Vol. 97, No. 4, pp. 1087–1096, 1978.

[34]   E. Bazelyan, "The leader of a long positive spark," Electr. Technol. USSR, 1987.

[35]   F. Rizk, "Switching impulse strength of air insulation: leader inception criterion," Power Deliv. IEEE Trans., Vol. 4, No. 4, pp. 2187–2195, 1989.

[36]   S. Gu, N. Xiang, J. Chen, W. Chen, S. Xie, and J. He, "3D Channel tortuosity of long air gap discharge," in 7th Asia-Pacific International Conference on Lightning (APL), 2011, pp. 784–787.

[37]   W. Mosch and E. Lemke, "Ein Modell zum Durchschlagprozess langer Luftfunkenstrecke," ETZ-A, Vol. 95, No. 5, pp. 256–260, 1974.

[38]   G. Aleksandrov and G. V. Podporkyn, "Analysis of experimental data on the electric strength of long air gaps," IEEE Trans. Power Appar. Syst., Vol. PAS-98, No. 2, pp. 597–605, 1979.

[39]   F. a. M. Rizk, "Critical switching impulse strength of long air gaps: modelling of air density effects," IEEE Trans. Power Deliv., Vol. 7, No. 3, pp. 1507–1515, Jul. 1992.

[40]   E. J. Los, "A model for the study of switching-surge breakdown of long air gaps," IEEE Trans. Power Appar. Syst., Vol. 97, No. 6, pp. 2382–2392, 1978.

[41]   I. Fofana and A. Beroual, "A predictive model of the positive discharge in long air gaps under pure and oscillating impulse shapes," J. Phys. D. Appl. Phys., Vol. 30, No. 11, p. 1653, 1997.

[42]   A. Bondiou-Clergerie and I. Gallimberti, "Theoretical modelling of the development of the positive spark in long gaps," J. Phys. D. Appl. Phys., Vol. 27, No. 6, pp. 1252–1266, 1994.

[43]   M. Becerra and V. Cooray, "Time dependent evaluation of the lightning upward connecting leader inception," J. Phys. D. Appl. Phys., Vol. 39, No. 21, pp. 4695–4702, 2006.

[44]   M. Becerra and V. Cooray, "A self-consistent upward leader propagation model," J. Phys. D. Appl. Phys., Vol. 39, No. 16, pp. 3708–3715, Aug. 2006.

[45]   L. Arevalo and V. Cooray, "On the interception of lightning flashes by power transmission lines," J. Electrostat., Vol. 69, No. 3, pp. 220–227, Jun. 2011.

[46]   L. Arevalo and V. Cooray, "'The mesh method' in lightning protection standards - Revisited," J. Electrostat., Vol. 68, No. 4, pp. 311–314, Aug. 2010.

[47]   H. Singer, H. Steinbigler, and P. Weiss, "A charge simulation method for the calculation of high voltage fields," IEEE Trans. Power Appar. Syst., Vol. 93, No. 5, pp. 1660–1668, 1974.

[48]   N. H. H. Malik, "A review of the charge simulation method and its applications," IEEE Trans. Electr. Insul., Vol. 24, No. 1, pp. 3–20, 1989.

[49]   A. Castellani, "Calcul du champ electrique par la methode des charges equivalentes pour la simulation d'une decharge bi-leader," 1995.

[50]   M. Becerra, "On the estimation of the charge of positive streamers propagating in air," IEEE Trans. Dielectr. Electr. Insul., Vol. 21, No. 2, pp. 627–634, 2014.

[51]   G. Maslowski and V. a. Rakov, "A study of the lightning channel corona sheath," J. Geophys. Res., Vol. 111, No. D14, p. D14110, 2006.

[52]   P. Ortéga, F. Heilbronner, F. Rühling, R. Díaz, and M. Rodière, "Charge–voltage relationship of the first impulse corona in long airgaps," J. Phys. D. Appl. Phys., Vol. 38, No. 13, pp. 2215–2226, Jul. 2005.

[53]   D. Wu, L. Arevalo, M. Li, and M. Larsson, "Switching Impulse Test of Large Sphere-Plane Air-Gaps with Protrusion on Large Spheres," Proc. 18th Symp. High Volt. Eng. ISH 2013, pp. 2334–2337.

[54]   S. Vibholm and P. Thyregod, "The analysis of insulation breakdown probabilities by the up-and-down method," IEEE Trans. Electr. Insul., Vol. EI-21, No. 2, pp. 133–136, 1986.

[55]   W. Hauschild and W. Mosch, Statistical techniques for high-voltage engineering, No. 13. 1992.

Acta Universitatis Upsaliensis

Digital Comprehensive Summaries of Uppsala Dissertations
from the Faculty of Science and Technology 1389

Editor: The Dean of the Faculty of Science and Technology